Cement & Concrete Composites 30 (2008) 907–916

Contents lists available at ScienceDirect

Cement & Concrete Composites

journal homepage: www.elsevier.com/locate/cemconcomp

Evaluating residual properties of thermally damaged concrete

Luigi Biolzi *, Sara Cattaneo, Gianpaolo Rosati

Department of Structural Engineering, Politecnico di Milano, Piazza L. da Vinci 32, 20133 Milano, Italy

ARTICLE INFO

Article history:
Received 28 September 2007
Received in revised form 1 September 2008
Accepted 4 September 2008
Available online 12 September 2008

Keywords:
High strength concrete
High temperature
Mechanical properties
Size effect
Fiber reinforcement

ABSTRACT

Detailed observations are presented on the evaluation of the residual properties of high strength concrete specimens after exposure to high temperatures. The variables considered were fiber reinforcement consisting of steel or polypropylene microfibers and two different specimen sizes. Both heat treated and undamaged (no heat treatment) specimens were tested by conducting three-point bending experiments at ambient conditions approximately one month after exposure to the high temperature. Residual strength and post-peak response were monitored using a closed-loop load frame, and the damage zone was observed with optical and acoustic techniques. Electronic speckle interferometry provided high resolution measurements of the displacement field due to the development of fracture. The size and shape of the localized damage zone were identified through the acoustic emission due to pre-peak microcracking, one of the significant factors influencing the strength of quasi-brittle materials.

1. Introduction

Concrete is commonly considered to have good fire resistance but chemical and physical reactions occur at elevated temperatures [1–6]. As a consequence, exposure to high temperatures may cause considerable variations in the physical and mechanical properties with irreversible loss of strength and stiffness, including the possibility of increased ductility in the post-peak regime [5–8]. This behavior is influenced by microcracking and spalling, generated by thermal incompatibility of the various components, the type of aggregate, heating rate, initial moisture content and permeability. For the cement matrix, thermal treatments to high temperatures cause a reduction in the amount of chemically bonded water in the hydrate phase. In particular, with an increase in temperature, gel-like hydration products are decomposed followed by a removal of hydroxide from the calcium hydroxide [9]. Therefore, significant changes in the microstructure of the material and, as a result, of properties of concrete may happen due to elevated temperatures.

The mechanical properties of a material are unique and should be independent of specimen size and shape. However, the common perception that concrete compressive and tensile strengths are inherent material properties is incorrect because the strength of a concrete specimen changes based on the specimen size [10]. Furthermore, with thermal treatment at elevated temperature, chemical/physical transformations in aggregates and paste are developed and many small pores and microcracks form within the concrete element. Since these micro-defects have a significant effect in defining the true residual strength of the material, it is necessary to perform analyses that remove from the nominal strength evaluated from a test, the influence of a given specimen size on the experimental data.

Residual mechanical properties have been studied extensively [5–7], including a numerical model of hydro-thermo-mechanical phenomena in heated concrete, treated as a multiphase porous material [11,12]. To assess residual mechanical properties, different procedures have been suggested and defined as the [7,13]

(1) stressed test method,
(2) unstressed test method,
(3) unstressed residual property test method.

The stressed and unstressed test methods are performed at elevated temperatures; concurrent loading and heating application are required. The unstressed residual property test method is employed to provide mechanical properties of concrete at room temperature after an elevated temperature treatment [13,14].

Nevertheless, residual properties are commonly detected by testing specimens of equal size, without any material identification and, among work reported in the literature, using dissimilar heating rates, specimen sizes and shapes, and loading configurations. Thus, these differences do not allow for a reliable evaluation of mechanical properties. Standard test methods should be defined in order to correctly evaluate, removing the size dependence, experimental findings on residual properties of concrete at elevated temperature [14].

The purpose of this paper is to present observations and extract some conclusions about the evaluation of the residual properties of specimens of two different sizes after exposure to high

* Corresponding author. Tel.: +39 02 2399 4314; fax: +39 02 2399 4220.
E-mail address: biolzi@stru.polimi.it (L. Biolzi).

0958-9465/$ - see front matter © 2008 Elsevier Ltd. All rights reserved.
doi:10.1016/j.cemconcomp.2008.09.005

temperatures. The variables considered for the high strength concrete were steel or polypropylene microfibers. It is well known that the steel fiber reinforcement enhances the mechanical properties whereas the polypropylene reinforcement is claimed to improve fire resistance; the polypropylene fiber easily melts and dissolves (at approximately 160 °C), creating additional pores and small channels in the concrete, which allows liquid and steam transport with the relaxation of the internal pressures in the heated material. Unstressed residual property tests were monitored with an interferometric technique referred to as electronic speckle pattern interferometry, which provides a map of the displacement field [15]. During the tests, the observation of fringes in real time on a monitor allowed a qualitative monitoring of the crack length at failure. In addition, the size and shape of the localized damage zone were identified through acoustic emission monitoring. The problem of evaluating the residual properties of thermally damaged concrete (and in fact, any quasi-brittle material) is specimen-size dependent, whatever is the geometry of the specimen and the load configuration.

2. Experimental techniques

2.1. Mix designs and test specimens

Mix-components of the cement-based materials used for this investigation can be summarized as follows: a Portland cement CEM I 52.5 R, according ENV 197/1 European Standard; an uncompacted grey microsilica; an acrylic copolymer superplasticizer, 30% solid content; a natural crystalline quartz of high purity (99% SiO_2), maximum aggregate size of 3 mm; brass coated carbon steel microfibers, diameter 0.15 mm, length 6 mm; monofilament type of polypropylene fibers, diameter 0.18 μm, length 6 mm. The concrete had an aggregate/binder ratio of 2 and a water/binder ratio of 0.22. The superplasticizer dosage, that is the ratio between the dry mass of superplasticizer solids and the mass of cement, was 0.02 for unreinforced material, increasing for the other materials in order to obtain the same workability. The microsilica/binder ratio was 0.1; the steel fiber (SF) contents were 0% and 2% by volume; the polypropylene (PF) fiber contents were 0% and 0.2% by volume. The mixture proportions of concrete mixes are shown in Table 1. The fiber contents by volume of concrete for each batch of specimens are listed in Table 2.

All specimens were prepared using steel molds and consolidated with a high frequency vibrating table, removed from the mold after 24 h, and cured in water at a temperature of 20 °C for one week and in air (20 °C and 90% R.H.) for three weeks. The maximum grain size of 3 mm improves efficiency of short fiber reinforcement and also increases accuracy of source locating by acoustic emission.

Table 1
Mixture proportions of concrete mixes

Aggregate/binder	2
Water/binder	0.22
Acrylic copolymer superplasticizer/cement	0.02
Microsilica/binder	0.1
Carbon steel microfibers (diameter 0.15 mm, length 6 mm) volume	0–2%
Monofilament type of polypropylene fibers, (diameter 0.18 μm, length 6 mm) volume	0–0.2%

Table 2
Fiber contents for each batch of specimens

Mix	Polypropylene fibers (%)	Steel fibers (%)
NF	0	0
PF	0.2	0
SF	0	2

2.2. Heating rates and furnace

An electric furnace was used for the thermal treatment; the maximum temperature reached was 750 °C. Intermediate temperatures were set at 250 and 500 °C. The ramps (Fig. 1a) were chosen in order to avoid high gradients. In this way, the specimens were warmed up to the fixed temperature at a speed of 1 °C/min, and after 2 h at the peak temperature, they were cooled at a speed of about 0.5 °C/min. The temperatures of the specimens are monitored by five K-type thermocouples. The change in colour that gives a visual indication of a significant modification in the concrete's properties, detected in the specimens is shown in Fig. 1b. The considered thermal treatment is consistent with proposed methods of assessment of fire resistance [13]. The specimens were not dehydrated prior to being heated and no spalling or explosion was observed at any of the concrete mixtures. Both undamaged and heat treated specimens were tested at ambient conditions approximately one month after exposure to the high temperature. Another variable that could affect the evaluation of residual properties for thermally damaged concrete includes the restoration of strength by re-hydration during the time between thermal exposure and testing. Indeed, it has been shown that the heated cement paste is not stable in the wet atmosphere and re-hydration processes take place [16].

2.3. Closed-loop testing

The testing system consisted of a closed-loop electromechanical Instron load frame with a maximum capacity of 100 kN. The main characteristics are as follows:

(1) electromechanical controls with a minimum speed of 2 μm/h;
(2) three control channels, one of which can be external (giving the possibility to choose the feedback signal that allows stable test control);
(3) closed-loop control with integral and derivative gain (in order to remove the effect of the finite stiffness of the machine).

To avoid unstable failure, strain control tests were performed with the choice of crack mouth opening displacements as the feedback signal to the servo-controller. The output of the transducers, including a load cell and strain gages, were automatically recorded using a data acquisition system. Furthermore, the load-deformation data were continuously displayed through the use of a personal computer.

2.4. Acoustic emission

The acoustic emission signals generated in laboratory specimens are captured using piezoelectric (PZT-5A) transducers attached to the specimen surface, and preamplified before recording. The sensors have a reasonably flat frequency response from 0.1 to 1 MHz and a sensor diameter of about 3 mm. They are mounted directly to the material with a methyl-cyanoacrylate glue and catalyst. Preamplifiers (40 dB gain) and filters (bandpass from 0.1 to 1.2 MHz) were chosen to maximize amplification, minimize noise, and assure matched frequency response. The data acquisition system consists of four, two-channel digitizers with a sampling rate of 20 million samples per second per channel (50 ns between two consecutive samples) and 8-bit resolution.

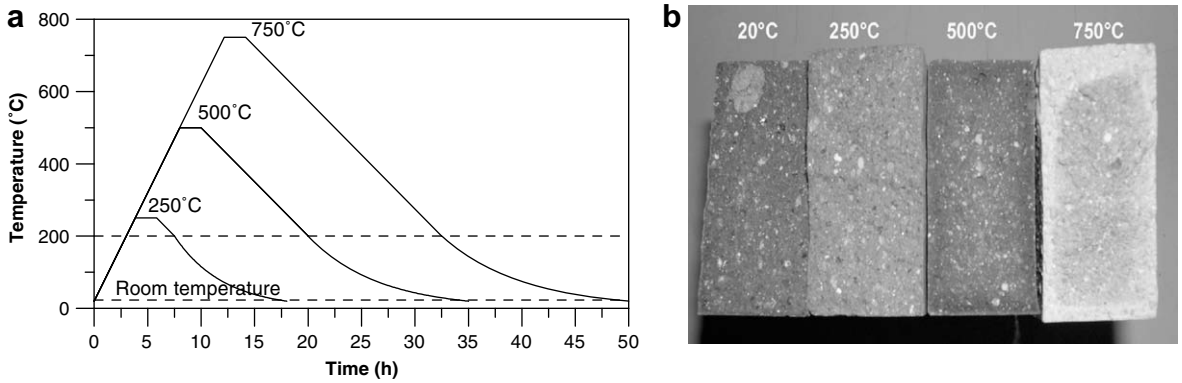

Fig. 1. (a) Thermal cycles and (b) change in colour after a thermal cycle.

The controller interfaces with a personal computer via a GPIB cable and an AT-GPIB card. The digitizers are equipped with an internal trigger that is activated whenever an AE signal exceeds the preset value. This threshold of amplitude must be set so that environmental noise does not trigger the system. The trigger-out signal of the first digitizer is fanned out to the other three digitizers for the acquisition to begin simultaneously at all the digitizers. One of the trigger-out signals is also sent to the load–displacement data acquisition system to correlate AE with the loading history.

In general, source location techniques involve a network of AE sensors positioned at different points on the specimen. Microseismic activity due to a change in stress is detected at each sensor at a given time. By knowing the relative arrival times of the P-wave, which is the component of the signal that arrives first, the P-wave velocity of the material, and the coordinates of each receiver, the event hypocenter can be estimated with a minimum of four sensors. Because some error is associated with arrival-time detection (it is not always clear when the signal arrives) and with the P-wave velocity measurement (as damage accumulates material properties may change or become anisotropic), the number of sensors should be increased so that the location problem becomes over-determined. In the present tests, eight piezoelectric transducers (Physical Acoustic model S9225) were arranged so that the fracture process zone was covered. Four sensors were located on the back face and four sensors were mounted on the front face of specimens. To perform the source location it is necessary to know the P-wave velocity.

2.5. Electronic speckle pattern interferometry

The electronic speckle pattern interferometry (ESPI) is an interferometric method used to measure a deformation field of diffusely scattering objects. ESPI is full field strain measurement technique with the following components employed in this paper:

(1) a Melles–Griot He–Ne laser (wavelength $\lambda = 632$ nm, $P = 30$ mW),
(2) a Panasonic WV BP310/G CCD camera,
(3) a DT-2861 frame grabber.

When an optically rough surface is illuminated by a laser beam, a random pattern of irregular or regular dots is observed. This phenomenon is called as laser speckle pattern. In this technique, two laser beams are used to illuminate the object, so that, by combining the object speckle and the reference beam, it is possible to obtain a brightness of the image speckle very sensitive to specimen movement.

3. Experimental results

3.1. Microscopic analysis

SEM investigations showed enhanced changes in the morphology as a consequence of exposure to high temperatures. Micrographs that reveal characteristics features of the undamaged materials after the exposure are shown in Figs. 2–4. In particular, a comparison between the untreated plain concrete and the same composition treated to 750 °C, is shown in Fig. 2a and b. Two SEM photographs of polypropylene fiber reinforced concrete before (Fig. 3a) and after 500 °C treatment (Fig. 3b) and of the steel fiber reinforced concrete before (Fig. 3c) after 750 °C treatment (Fig. 3d) are showed in Fig. 3. Detailed images of the treated steel fibers are shown in Figs. 4a and 4b.

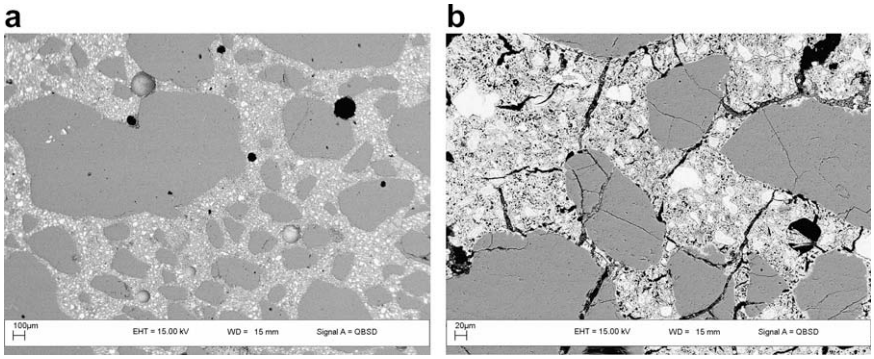

Fig. 2. SEM analysis plain concrete: (a) 20 °C and (b) 750 °C.

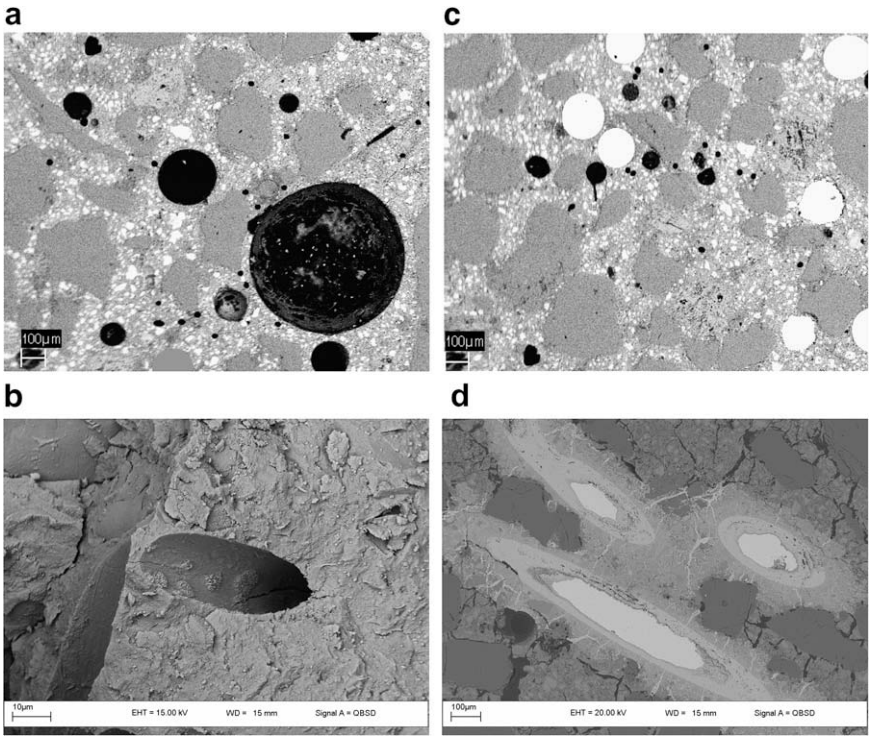

Fig. 3. SEM analysis: polypropylene fiber reinforced concrete (a) before test, and (b) after exposure to 500 °C, and steel fiber reinforced concrete (c) before test, and (d) after exposure to 750 °C.

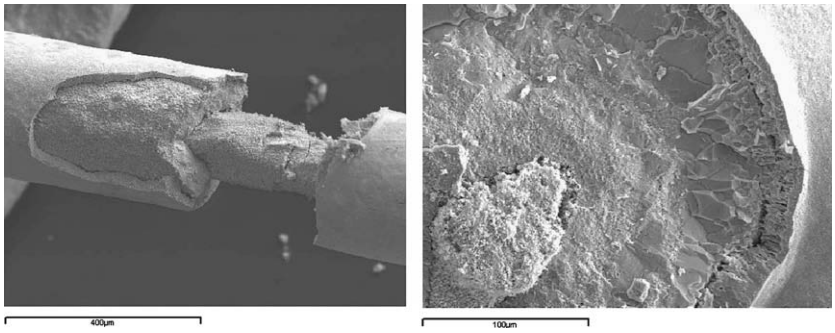

Fig. 4a. Single steel fiber exposed at 750 °C.

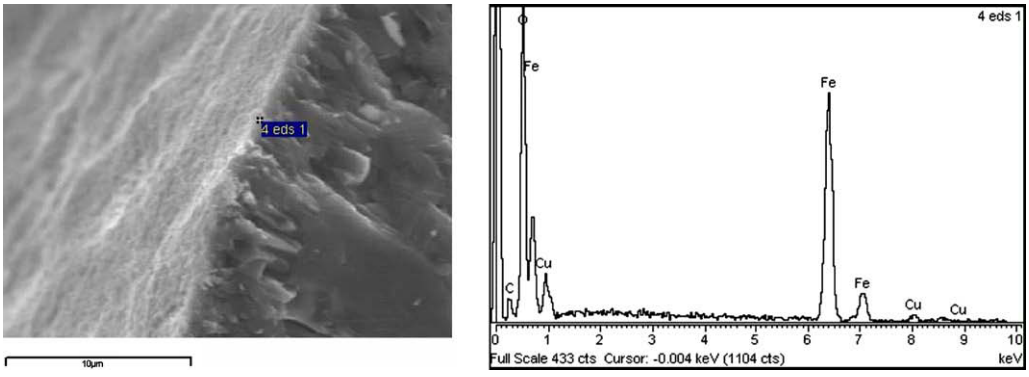

Fig. 4b. EDS analysis performed on the surface of fractured oxidized fiber at 750 °C.

The concrete with polypropylene fibers at 500 °C showed an absence of fibers completely melted and vaporized (Fig. 3b). The specimens exposed to 750 °C revealed serious changes in the morphology, characterized by diffuse microcracks across both the aggregate and cement paste. In addition, a tendency appeared for microcracks to develop with an orientation parallel to the

specimen boundaries. The increase in microcracking was evident by examining the increased porosity, permeability and poor mechanical properties. When the temperature reached 750 °C, the steel fibers, partially melted, tend to fill the cracks formed in the concrete. An exchange of material between the external portion of steel fibers and concrete paste took place, as confirmed by the presence of calcium and silica in the fibers. SEM and EDS analyses on single steel fibers (Figs. 4a and 4b) revealed that fiber partial melting occurred and the internal core of fibers is clearly different from the external portion in terms of both morphology and composition. Furthermore, the X-ray diffractometer demonstrated that the fibers were completely oxidated and, as a consequence, characterized by a significant reduction in mechanical properties [17]. The EDS analysis, performed on the surface of fractured oxidized fiber, confirmed the presence of iron, oxygen and copper (Fig. 4b).

3.2. MIP results

Porosimetric data – cumulative volume (cm^3/g) and total porosity (%) – are summarized in Figs. 5a and 5b [15]. In general, the addition of fibers was responsible for a slight increase of porosity, with temperature to 500 °C. A significant increase in porosity was observed after heating at 750 °C, confirming an enhanced material degradation that can have an effect on the mechanical properties. In particular, with reference to undamaged concrete, the porosity values doubled more than with an exposure to 750 °C.

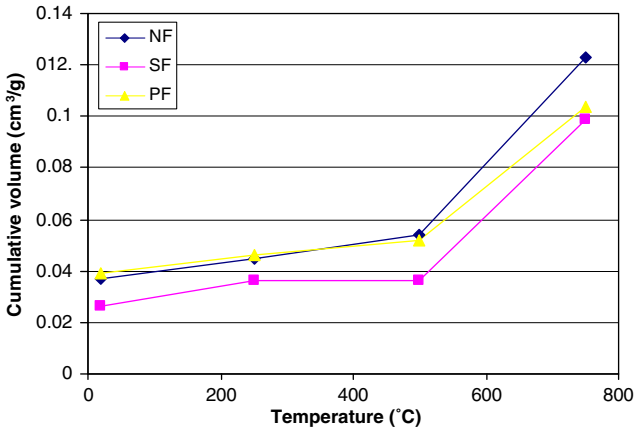

Fig. 5a. Cumulative volume.

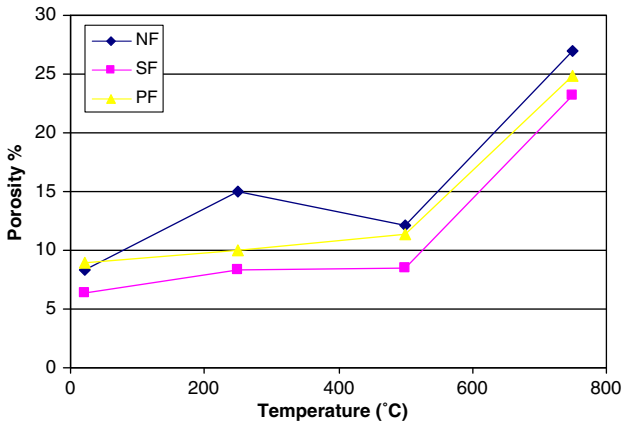

Fig. 5b. Porosity.

3.3. Residual mechanical properties

3.3.1. Bending tests

To determine the fracture properties under various heating scenarios, three-point bending tests were performed on preheated concrete beams of dimensions $500 \times 100 \times 30$ mm (L-specimens) and $300 \times 50 \times 30$ mm (S-specimens). The effective span of the beams was 400 and 250 mm, respectively. Typical bending stress–displacement curves for specimen of larger dimensions made of different mixtures and for a given thermal cycle are shown in Fig. 6 together with crack pattern observed at peak load on the surface of the specimens; arrows indicate the crack tip. Softening of concrete is apparent with increasing temperature. This can be demonstrated with an objective comparison of the overall response considering normalized load–displacement curves (dividing the loads and displacements by the corresponding values at failure). Whereas in the pre-peak branch, the shapes of the curves are similar, in the post-peak part of the normalized load–displacement curves, the influence of thermal treatment is apparent: the decreasing load-carrying capacity becomes less critical with the increasing of severity of thermal treatment [8,21].Fig. 7 shows the ESPI images at peak load for specimens of dimensions $300 \times 50 \times 30$ mm.. As a consequence of thermal damage, in the pre-peak range, a definite evolution in the hardening regime was observed and this, in the end, defines the strength of a material as well as scaling of strength and fracture energy. Noteworthy differences in the damage progression were monitored for the two considered geometries. In particular it can be observed that the ESPI images at peak load suggested a dissimilar strain field and therefore a clear influence of specimen size. The crack penetration at peak load (Fig. 8a) was almost constant for undamaged and heated specimens. A noteworthy difference has been observed in the large steel fiber reinforced specimen, where crack penetration at peak load decreased perhaps also because of local breakdowns in bond between the cement and the reinforcement. This behavior was not observed for the small steel fiber reinforced specimens. However, an enhanced difference was noted for the onset of fracture detected by the ESPI observations (first discontinuity in ESPI fringes). The ratio between the loads at onset of fracture and at peak (load ratio) as a function of the maximum temperature of the thermal cycles is shown in Fig. 8b: with the increasing of severity of thermal treatment, the localization was detected at decreasing load ratio levels. Thus, longer hardening regime characterized the heat treated specimen. It is interesting to compare the crack length at peak load with the corresponding AE locations (Fig. 9). The AE locations appear more deeply diffused in the beams, denoting a large process zone ahead of the crack tip. The evolution of the AE activity occurred around the middle cross section of the beam, the site of tensile failure. At peak stress, the microcracks concentrated in a narrower region spread from the bottom of the specimen. With the increase in the severity of heating, this microcracked region grew in length and width (Fig. 9). The strain and/or stress gradients, that cannot be disregarded from any analysis of experimental data, appeared less pronounced. A comparison between specimens made of plain and polypropylene fibers reinforced concrete (concrete of similar apparent strength) showed that this evolution was slightly more accentuated with fiber reinforced specimens where the AE activity, at peak load, was diffused on a larger volume.

In the case of steel fiber-reinforced specimens, prolonged AE activity was measured and discontinuities of ESPI fringes, indicating multiple cracks, were observed.

The experimental evidence clearly showed that, as a consequence of thermal treatment the strain field at peak load, was perceptibly different in the specimens and in particular in the critical

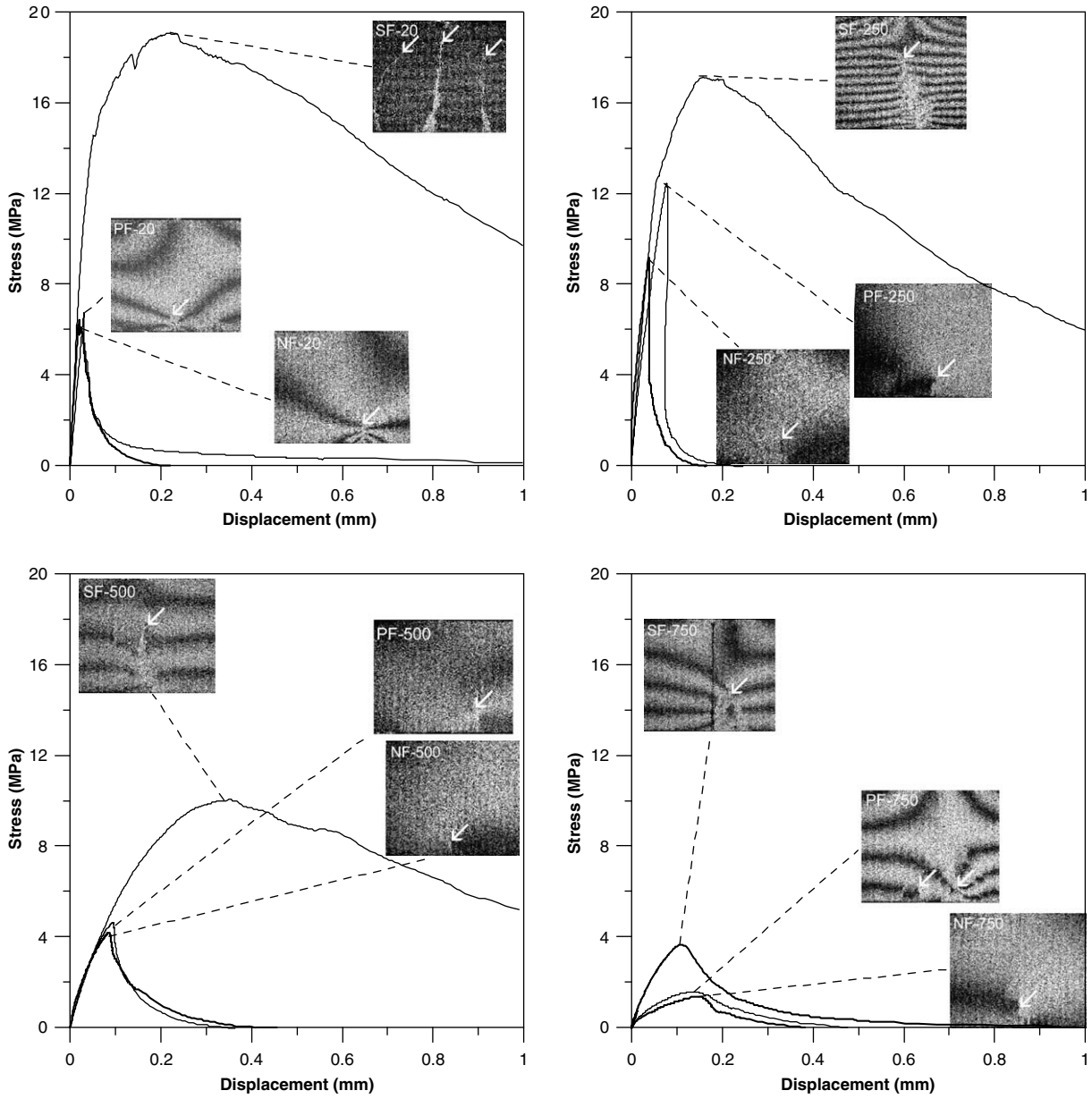

Fig. 6. Typical bending stress – displacement curves for large specimens together with ESPI images observed at the peak load (white arrow indicates the crack tip).

cross section where the coalescence process of microcracks results in a main crack causing the final rupture of it.

Thus, the stress distribution is altered due to the microstructural differences generated in the material by the thermal damage. The differences affected the overall response of the specimens and in particular the bending tensile strength or modulus of rupture, captured from the flexure formula:

$$\sigma_N = \frac{M_{\max}}{S}, \tag{1}$$

where $M_{\max}$ is the maximum moment at peak load and S is the elastic section modulus.

Fig. 10 shows the bending strength as a function of the maximum temperature of the thermal cycles. For the range of temperatures considered in this study, all bending strengths underwent a two-stage process. In the first stage, these strengths either changed very little or slowly decreased with temperature until a transition point was reached. In the second stage, the strengths rapidly decreased with the severity of thermal treatments. This transition point is around 250 °C. For the considered materials, the concrete bending strengths change little at the lower temperatures and consequently, during this physical process, the removal of capillary water would not cause a significant reduction in the concrete strengths. There is no significant change in concretes up to a temperature of 300 °C in aggregate and mortar phases, but there are significant changes in aggregate and mortar phases after this temperature.

3.3.2. Compressive loading

All tests were carried out on concrete cylinders of 10 cm diameter × 20 cm height, and were cured under water at room temperature until test time. Before testing, the cylinders were removed from the curing tank and the ends were ground to be plane and perpendicular. The experimental results are summarized in Fig. 11. Similarly to bending strength, creation of pores and cracks resulting from physicochemical changes in cement paste and

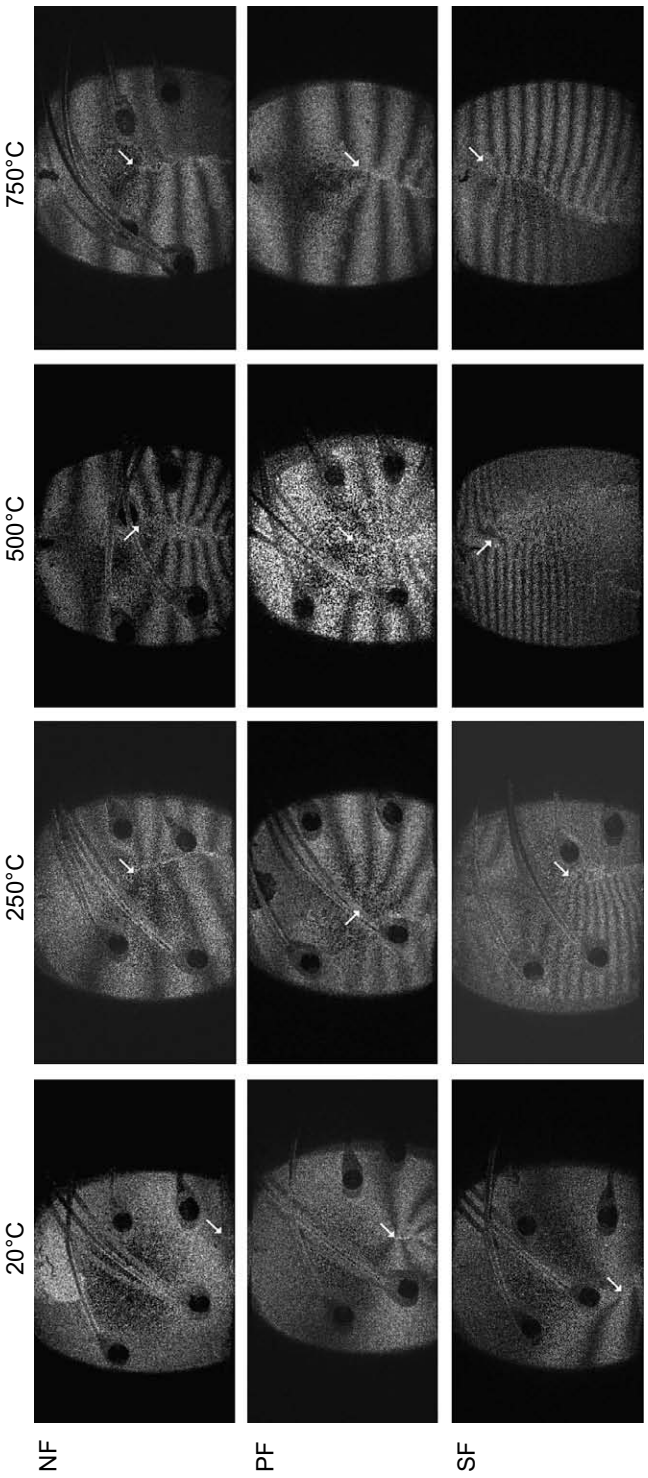

Fig. 7. ESPI images for small specimens at the peak load (the black circles are AE sensors).

thermal incompatibility between aggregate and cement paste caused deterioration in compressive strength of heated concrete.

3.3.3. Ultrasonic pulse velocity

Fig. 12 shows the concrete deterioration through ultrasonic pulse velocity (UPV) measurements. The UPV value, an additional indicator of damage, has been used successfully to evaluate the quality of concrete, as UPV is sensitive to degradation phenomena including internal cracking and other deterioration due to a thermal treatment [18–19]. The UPV value, after 250 °C, decreases almost linearly as the maximum heating temperature increase. Note that velocities of around 4500 m/s were measured after a single cycle up to 250 °C, but values less than 2000 m/s were measured in specimens heated to 750 °C. Young's modulus of the concrete had a similar trend, with a monotonically decrease with increasing heating temperature after 250 °C. Up to 250 °C, it is known that a possible reduction is mainly influenced by the volume of the evaporated capillary water and this was not important for the tested concrete. In any case, the degeneration of the elastic properties of the individual ingredients is noteworthy at higher temperatures. Therefore, in evaluating the deformation of thermally-damaged concrete structures, it is imperative to take into account the effect of temperature on the elastic modulus too.

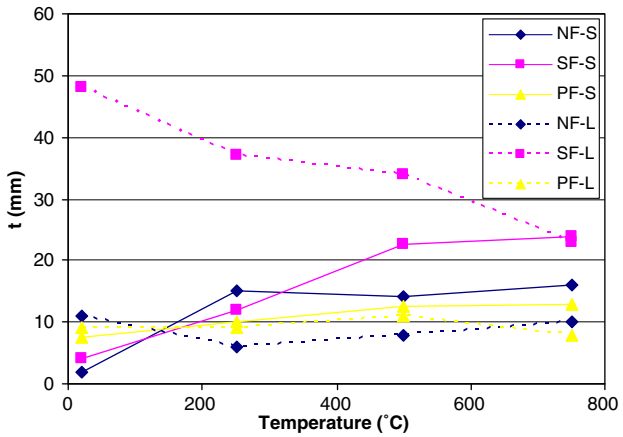

Fig. 8a. Crack penetration t at peak load.

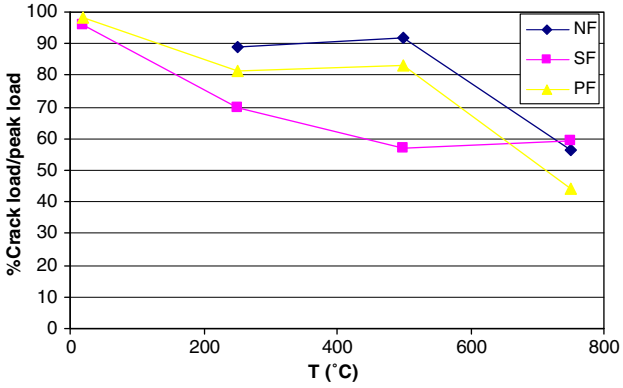

Fig. 8b. Load ratio as a function of the maximum temperature.

4. Discussion

With heat treatment to high temperatures, profound and irreversible transformations in the material must be considered to analyze the problem of residual properties in bending. Testing thermally damaged specimens of equal geometry, the experimental evidence showed that the population of microcracks evolves (in number and size of cracks) and depends also on alterations in the material due to heating. Crack propagation in concrete specimens is therefore accompanied by a process zone of variable size. Due to heating scenario, a diverse evolution of residual strength with size results, that is, the damage process detected in the specimens, that has a fundamental influence on size effects, influence a correct

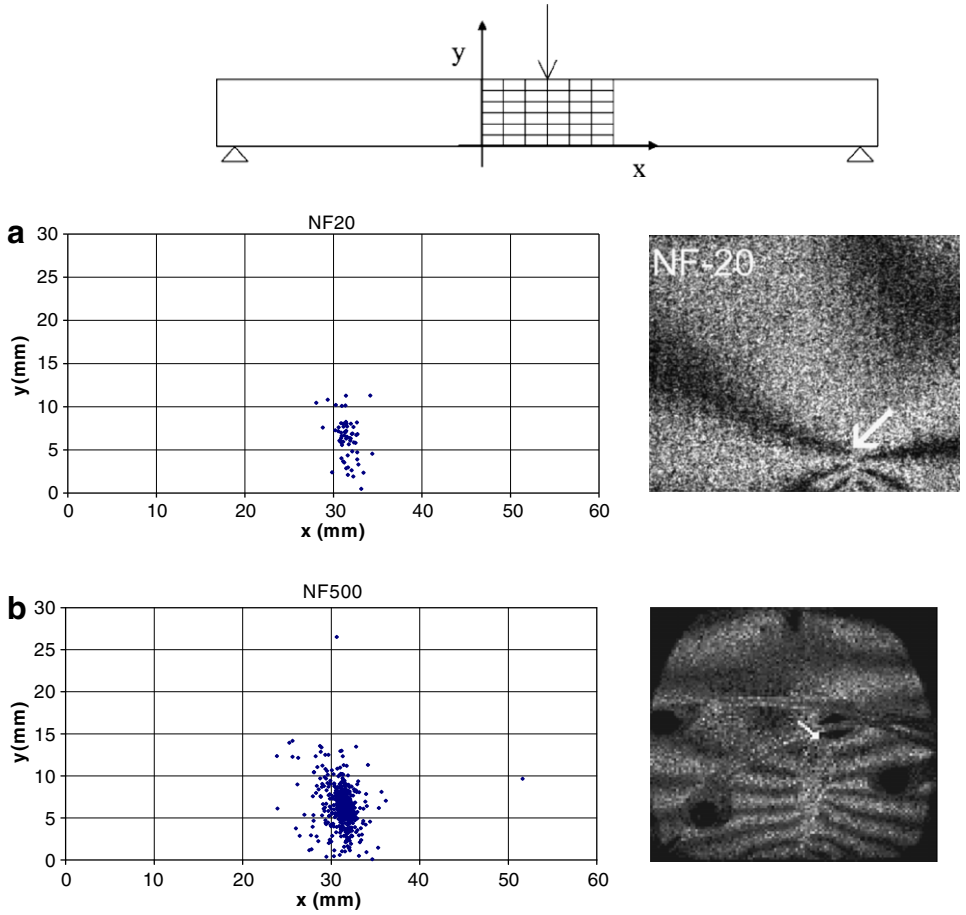

Fig. 9. Locations of acoustic emission and ESPI images at the peak load for (a) undamaged specimen and (b) thermally damaged specimen (single cycle at 500 °C).

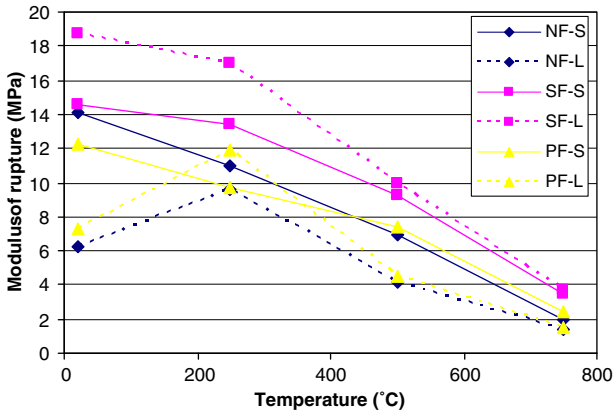

Fig. 10. Bending strength as a function of the maximum temperature.

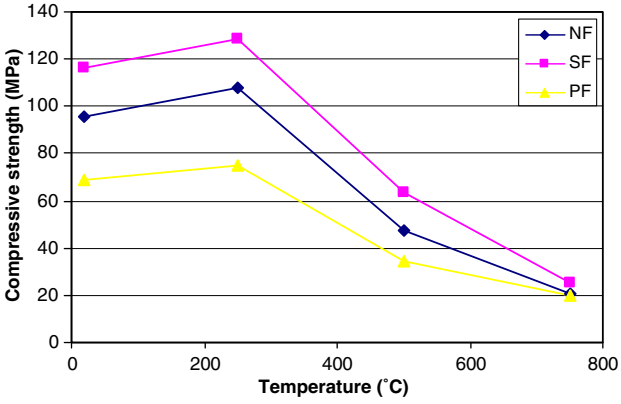

Fig. 11. Residual compressive strengths – Small specimens.

assessment of true mechanical properties because the specimens can be considered made with a different material.

A mechanical approach to the problem of bending strength [20–21], is to consider a substitution of the microcracked volume where the AE activity at peak load is localized with a opportune cohesive interaction applied to a notched specimen (Fig. 13). The notch is a consequence of the intrinsic process zone and this notched specimen controls the peak stress.

Acoustic emission locations show that a small volume becomes further microcracked upon reaching peak stress. For a typical specimen, the volume of the intrinsic process zone is orders of magnitude smaller than the volume of the specimen. To capture the essential behavior, some simplification of the problem may be justified with respect to the geometry of the process zone and its cohesive interaction. If the radius of curvature of the notch (ρ) is taken to be one-half the width of the intrinsic process zone and the failure criterion adopted is that at peak load the stress at the notch tip reaches the "true" or theoretical residual tensile strength σ_{rt},

$$\sigma_{rN} = \sigma_{rt}\frac{H}{h}F\left(\frac{h}{\rho}\right), \tag{2}$$

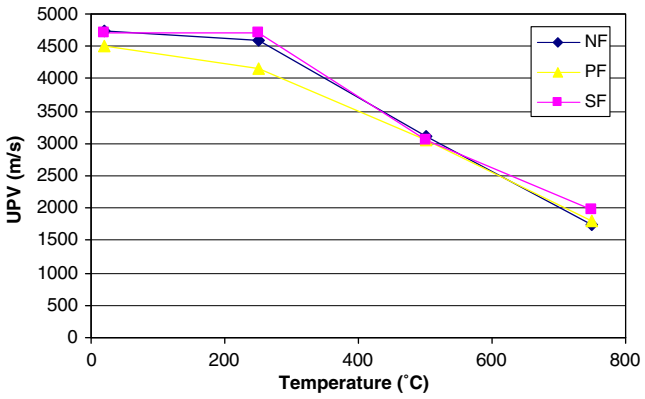

Fig. 12. Ultrasonic pulse velocity measurements as a function of temperature.

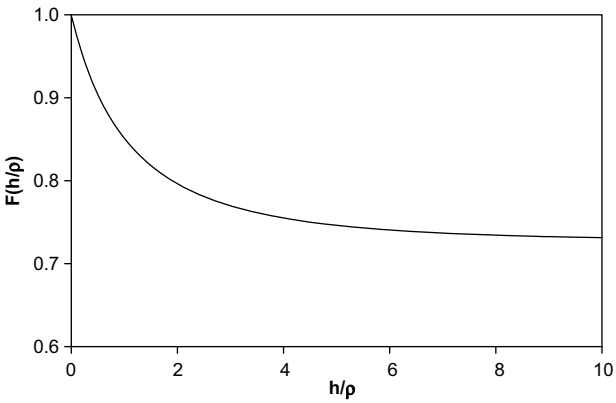

Fig. 14. Reduction coefficient (ρ radius of the microcracked volume at notch tip).

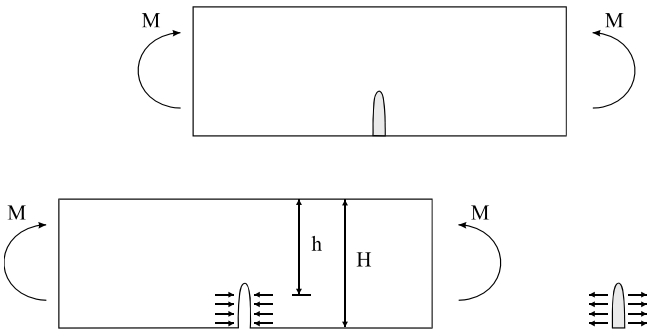

Fig. 13. Mechanical model.

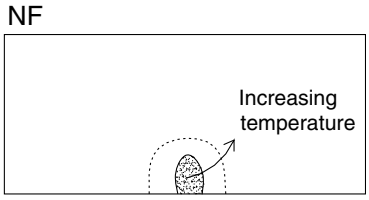

Fig. 15. Effect of thermal treatments on the microcracked volume at peak load.

where σ_{rN} is the nominal strength defined by relation (1). Note that the nominal strength depends not only on the theoretical tensile strength of the material, but also on

(a) the cohesive interaction, as measured by the ratio between the beam height H and the undamaged ligament h and
(b) the notch effect induced by the intrinsic process zone, as measured by the function $F(h/\rho)$ that depends on the undamaged ligament h and the radius of the notch tip ρ defined by the microcracked volume.

Indeed, the two factors compete in defining the bending strength of a concrete beam. The ratio H/h is the amplification factor due to the cohesive interaction of the process zone, whereas $F(h/\rho)$ is the reduction coefficient that represents the perturbation in the stress field due to the shape and size of the undamaged volume. A plot of $F(h/\rho)$ is shown in Fig. 14: $F(h/\rho)$ is 1 when $F(h/\rho)$ h/ρ tends to 0 (no notch in the beam) and for values of h/ρ greater than 10, the function reaches an asymptotic value approximately equal to 0.74. The ratio H/h is always greater than 1 and it is the measure of the positive contribution of the microcracked process zone to the bending strength.

After a thermal treatment the material becomes less brittle (the intrinsic length increases), the specimen size that is needed to determine the lower limit of the nominal strength for a given test geometry must increase. In any case, both the two contributions in (2) have a positive effect to increasing severity of the thermal treatment: cohesive effect increases and the notch effect is reduced (Fig. 15). It is possible to assert that the inelasticity of the process zone tends to be dominant with respect to the notch effect. For steel fiber-reinforced specimens, the notch effect is nonexistent due to multiple cracking and the pre-peak extended AE activity.

Hence evaluating residual property considering identical specimens and applying the relations of the classic beams theory may cause an underestimation of the effective or true residual strength of the material. The important distinction is in the pre-peak microcracking, which influences the strength of a specimen, and with that the scaling of strength.

It is important to realize that after heat treatment, the specimens have an altered constitutive behavior. In this context, an understanding of the failure process of the quasi-brittle material is decisive for a correct interpretation of the experimental data. Therefore, a suite of experiments should be conducted to find the intrinsic residual properties that are independent of specimen size. For example, the experiments should include:

(a) appropriate monitoring to detect the characteristics of the microcracked volume at the peak load [20] and
(b) specimens of different sizes, but geometrically similar, to identify a true residual strength of the damaged material, by taking into account the size effect on nominal strength [10].

5. Conclusions

Evaluating mechanical properties with tests on specimens of equal size may cause significant underestimation of residual strengths, especially in specimens made with plain concrete.

Pre-peak microcracking in the damaged volume, which causes a nonlinear response, is one of the significant factors influencing the residual strength of concrete specimens.

The experimental results showed that the discontinuity in the ESPI fringes (crack initiation at peak load) tend to increase for heated specimens, characterized by a significantly greater hardening regime. With an enhancement in the severity of thermal treatment, the damage detected by the acoustic emission locations showed a tendency to increase, both in depth but more appreciably in the longitudinal direction (notch effect tends to decrease).

The size effect on residual bending tensile strength (modulus of rupture) is significant in the case of specimens made of plain or polypropylene fiber-reinforced concrete.

The multiple cracking and the pre-peak acoustic emission activity observed in steel fiber-reinforced specimens may cause a reduced influence of specimen size on the evaluation of the mechanical properties when considering identical specimens.

Acknowledgments

The authors wish to extend their gratitude to Prof. Luca Bertolini and Dr Gian Luca Guerrini various helps concerning the experimental program. This paper was written during a stay at Department of Civil Engineering of the University of Minnesota. Special thanks to Prof. J.F. Labuz for useful discussions. The Authors wish to acknowledge partial support of this research by the Italian MIUR under PRIN program.

References

[1] Lea FC. The effect of temperature on some of the properties of materials. Engineering 1920;110(3):293–8.
[2] Lea FC, Stradling R. The resistance to fire of concrete and reinforced concrete. Engineering 1922;114(4):341–4.
[3] Malhotra HL. The effect of temperature on the compressive strength of concrete. Mag Concrete Res 1956;8(22):85–94.
[4] Schneider U. Concrete at high temperatures – a general review. Fire Safety J 1988;13(1):55–68.
[5] Phan LT, Carino NJ. Review of mechanical properties of HSC at elevated temperature. J Mater Civil Eng ASCE 1998;10(1):58–64.
[6] Khoury GA. Effect of fire on concrete and concrete structures. Prog Struct Eng Mater 2000;2(4):429–47.
[7] Castillo C, Durrani AJ. Effect of transient high temperature on high strength concrete. ACI Mater J 1990;87(1):47–53.
[8] Labuz LF, Biolzi L, Chen CN. Estimating thermal damage and its influence on fracture toughness. In: Lutes LD, Niedzwecki JM, editors. Proc IX Conf Eng Mech. New York: ASCE; 1992. p. 523–6. 0-87262-867-1.
[9] Janotka I, Mojumdar SC. Thermal analysis at the evaluation of concrete damage by high temperatures. J Therm Anal Calorim 2005;81(1):197–203.
[10] Karihaloo BL. Fracture mechanics and structural concrete. Essex: Longman Publishing Group; 1995.
[11] Willam K, Rhee I, Xi Y. Thermal degradation of heterogeneous concrete materials. J Mater Civil Eng ASCE 2005;17(3):276–85.
[12] Schrefler B, Khoury GA, Gawin D, Majorana CE. Thermo-hydro-mechanical modelling of high performance concrete at high temperatures. Eng Computation 2002;19(7):787–819.
[13] Phan LT, Carino NJ. Code provisions for high strength concrete: strength–temperature relationship at elevated temperatures. Mater Struct 2003;36(256):91–8.
[14] Phan LT, Carino NJ. Effects of test conditions and mixture proportions on behavior of high-strength concrete exposed to high temperatures. ACI Mater J 2002;99(1):54–66.
[15] Packman PF. Experimental techniques in fracture mechanics, vol. 2. Ames (IA): Iowa State University Press; 1975.
[16] Alonso C, Fernandez L. Dehydration and rehydration processes of cement paste exposed to high temperature environments. J Mater Sci 2004;39(10):3015–24.
[17] Biolzi L, Guerrini GL, Bertolini L. Cementitious materials with hybrid fibers exposed to high temperatures. In: di Prisco M, editor. Proceedings sixth Rilem symposium on fibre reinforced concrete (FRC). Bagneaux: Rilem Press; 2004. p. 635–46.
[18] Popovics JS. Analysis of the concrete strength versus ultrasonic pulse velocity relationship. Mater Eval 2001;59(2):123–9.
[19] Naik TR, Malhotra VM, Popovics JS. The ultrasonic pulse velocity method. In: Malhotra VM, Carino NJ, editors. Handbook on nondestructive testing of concrete. Boca Raton: CRC Press; 1990. p. 169–88.
[20] Labuz JF, Biolzi L. Characteristic strength of quasi-brittle materials. Int J Solids Struct 1998;35(31–32):4191–204.
[21] Biolzi L, Labuz JF. Size effects in fracture of quasi-brittle materials. In: Aliabadi MH, editor. Nonlinear fracture & damage mechanics. Southampton: WIT Press; 2001. p. 201–23.